Adsorption (2012) 18:13–22
DOI 10.1007/s10450-011-9375-x

Investigation of hydrogen and methane adsorption/separation on silicon nanotubes: a hierarchical multiscale method from quantum mechanics to molecular simulation

Sahra Balilehvand · Seyed Majid Hashemianzadeh · SeyedehSaleheh Razavi · Hedayat Karimi

Received: 17 May 2011 / Accepted: 12 September 2011 / Published online: 13 October 2011

Abstract A combination of ab initio quantum mechanical (QM) calculations and canonical Monte Carlo (CMC) simulations are employed to investigate possible usage of single-walled silicon nanotubes (SWSiNTs) as a novel media for hydrogen and methane adsorption as well as their separation from each other. By fitting the force field, a Morse potential model is selected as an efficient potential to describe the binding energies between both hydrogen-SiNTs and methane-SiNTs obtained from ab initio calculations. Then CMC simulations are performed to evaluate the adsorption and separation behaviors of H_2 and CH_4 on the three different sizes of SiNTs including (5, 5), (7, 7), and (9, 9) SiNTs at ambient temperatures and pressures from 1 up to 10 MPa. As a comparison, the adsorption and separation of H_2 and CH_4 on the (8, 8) CNTs which are isodiameter with (5, 5) SiNTs are also simulated. Results are indicative of remarkable enhancement of H_2 and CH_4 adsorption capacity on the SiNTs compared to the CNTs, which arise from stronger van der Waals (VDW) attractions. In the case of methane adsorption on SiNTs, the stored volumetric energy exceeds the goal of the US Freedom CAR Partnership by 2010, which can not be achieved by methane compression at such low pressures. Moreover, simulation results indicate that SiNTs preferentially adsorb methane relative to hydrogen in their equimolar mixture, which results in efficient separation of these gases from each other at 293 K.

Keywords Silicon nanotube (SiNT) · Canonical Monte Carlo simulation · Morse potential · Gas adsorption · Gas separation

S. Balilehvand · S.M. Hashemianzadeh (✉) · S. Razavi · H. Karimi
Molecular Simulation Research Laboratory, Department of Chemistry, Iran University of Science & Technology, Tehran, Iran
e-mail: hashemianzadeh@iust.ac.ir

S.M. Hashemianzadeh (✉)
e-mail: hashemianzadeh@yahoo.com

S. Balilehvand
e-mail: sahra_balilehvand@yahoo.com

1 Introduction

The tremendous exploitation of the fossil fuels as the result of growing population and industrialization has had many serious consequences such as air pollution and global warming over recent years. Moreover, the reserves of fossil fuels are limited. Therefore, finding new energy sources is indispensable. Since H_2 and CH_4 are sustainable clean energy sources with high heat of combustion, they seem to be the eternal solution to eliminating pollution and the diminution of traditional sources (Zhang 2006; Zhou et al. 2005). However, regarding their considerable advantages, these energy sources have not been used extensively yet. The major impediments in this area are related to storage and transportation of these gases in a safe and economical way. Therefore, for H_2 and CH_4 storage, several alternative ways have been considered such as gas compression, liquefaction, and adsorption on solid state materials (Kowalczyk et al. 2006; Morales-Cas et al. 2007).

Danger of explosion and high weight of the gas storage vessels are the two limitation factors for on-board application of compression technique. Moreover, for CH_4 and H_2 liquefaction, the extremely difficult condition of low temperature is required because of their low critical temperatures (119 K for CH_4 and 33 K for H_2). Therefore, among the methods mentioned, adsorption is a promising technology if an appropriate adsorbent is accessible (Peng et al. 2008).

The separation of hydrogen and methane from each other is another issue that is of crucial importance, since 95% of hydrogen used in the fuel cells is provided by the purification of synthetic gas obtained from steam reforming of natural gas (Kowalczyk et al. 2007).

For more than two decades, a large variety of porous materials for instance carbon nanotubes (Tanaka et al. 2005; Poirier et al. 2006; Chen and Sholl 2006), fibers and activated carbon (Dillon et al. 1997; Bhatia and Myers 2006), molecular sieves (Ohkubo et al. 2002; Roussel et al. 2006), layered pillared pore materials (Cao et al. 2002), and metal organic frameworks (MOFs) (Li and Yang 2005, 2006) have been explored to find efficient adsorbent for H_2 and CH_4 storage, and their separation from each other. Carbon nanotubes have particularly attracted a great deal of attention because of their unique properties. Bekyarove et al. (2003) have reported measurement of methane adsorption on single-walled carbon nanotube (SWCNTs). In 2004, Lan et al. (2008) performed grand canonical Monte Carlo simulation (GCMC) to optimize the SWNT arrays for methane storage, and their simulation results demonstrated that methane storage in the optimized triangular arrays at 4.1 MPa exceeded the US Department of Energy (DOE) goal. Lee et al. (2006) have measured the methane adsorption on multi-walled carbon nanotubes (MWCNTs) compared to two types of zeolites (DAY and HSZ-320). Their experimental data indicated that the methane uptakes of MWCNTs were higher than for zeolites. Kowalczyk et al. (2006) have investigated methane storage on bundles of (10, 10) CNTs and worm-like carbon porous by GCMC simulation. Their results have revealed that such nanoscale materials can attain the US freedom CARP partnership goal at ambient temperature.

Many studies have also been accomplished about hydrogen adsorption on pristine and improved doped carbon nanotubes. However, most of these efforts have failed to attain the DOE target, namely 6.5 wt% by 2010. Nowadays, most of the researchers believe that the solution to this problem comes from the design of novel materials (Cote et al. 2005; Rosi et al. 2003; Yaghi et al. 2003; Mpourmpakis et al. 2006). Recently, silicon nanotubes (SiNTs) have been synthesized by several methods such as the chemical vapor deposition (CVD) (Sha et al. 2002) and hydrothermal (Chen et al. 2005; Tang et al. 2005) methods. Silicon is more polarizable than carbon due to the presence of more electrons in its outer shells. Therefore, we anticipate that SiNTs can be tailored to achieve a stronger van der Waals attraction to adsorbed molecules than CNTs (Lan et al. 2008). Only a few studies have been implemented about hydrogen adsorption on SiNTs (Lan et al. 2008; Lithoxoos et al. 2008; Ryou et al. 2008). Lan et al. (2008) have used multiscale theoretical method, combining the first-principle calculations and a grand canonical Monte Carlo (GCMC) simulation to evaluate the hydrogen adsorption on the SiNT arrays. They have found that capacity of hydrogen adsorption on SiNT arrays is considerably higher than that on CNTs and SiCNTs.

In the current study, we employed a multiscale theoretical approach to explore the hydrogen and methane adsorption on SiNTs as well as their separation from each other. First the binding energies between adsorbate and adsorbent obtained from ab initio calculations were fitted to a proper potential function. Then the results were applied as an input in the canonical Monte Carlo (CMC) simulation to evaluate capacity of adsorption of hydrogen, methane, and their equimolar mixture on SiNTs at different pressures, temperatures, and tube sizes. The amount of H_2 and CH_4 adsorption on SiNTs and CNTs were also compared. Lastly, the possibility of H_2–CH_4 separation by SiNTs was considered at 293 K.

2 Models and methodology

2.1 Ab initio calculations

In this section, for the determination of the interaction potential of CH_4 and H_2 with SiNTs, ab initio calculations were carried out using the Gaussian 03 program package.

Three different sizes of armchair-type SiNTs including (5, 5), (7, 7), (9, 9) SiNTs were adopted as adsorbents, due to survey of curvature effect on the adsorption behavior of species. In this work, to obtain results with high accuracy, without executing heavy calculations, the SiNTs were characterized by cluster model, since adsorbed molecules mainly interact with their closest atoms in the adsorbent (Mpourmpakis et al. 2006; Lan et al. 2008). According to the diameter of the tubes, two cluster models were used in the first-principle calculation. As shown in Fig. 1, the cylinder cluster model containing 70 Si atoms was chosen for the (5, 5) SiNT, because of its small diameter, whereas, for both (7, 7) and (9, 9) SiNTs, a graphite like sheet constituting 24 Si atoms were selected, due to their bigger diameters and lower curvatures. In addition, to avoid the edge effect, all the dangling bonds at the ends of the tubes were terminated by hydrogen atoms (Mpourmpakis et al. 2006; Meng et al. 2007). In all the selected cluster models of nanotubes, three adsorption sites were considered: on-top, bridge, and hollow (Lan et al. 2008). To find the energetically favorable site for H_2 and CH_4 adsorption, the binding energies were calculated in the mentioned positions, by DFT/MP1PW91 method, which could afford more accurate results than DFT/B3LYP for dispersion force (Mpourmpakis et al. 2006; Lan et al. 2008). Additionally, to attain the highest possible accuracy, for hydrogen, methane and their closest six silicon atoms, the 6-311++g** basis set was used, while for the other atoms, the 3-21g basis set was treated (Mpourmpakis et al. 2006;

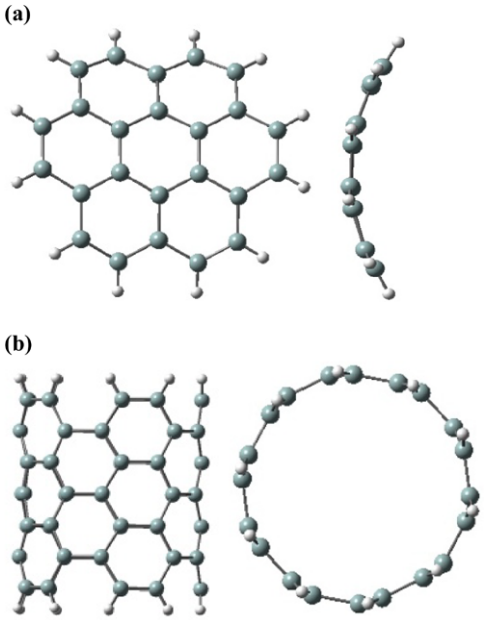

Fig. 1 Top and sideview of the SiNT cluster models where dangling bond at the end of tubes are saturated by hydrogen atoms: (**a**) (9, 9) SiNT and (**b**) (5, 5) SiNT

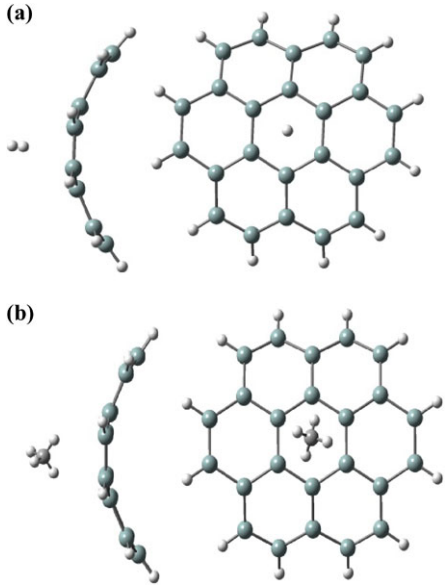

Fig. 2 The energetically favorable orientations for hydrogen and methane adsorption on the (7, 7) SiNT: (**a**) hydrogen adsorption and (**b**) methane adsorption

Lan et al. 2008). Our results indicate that the hollow sites are the most favorable adsorption sites for both H_2 and CH_4. It should be mentioned that similar results have also been obtained for adsorption of hydrogen on SiNTs by Lan et al. (2008).

According to the results obtained from geometry optimization, the hollow sites were considered to perform potential energy surface scans. Many different orientations were possible when H_2 and CH_4 approached the hollow sites of the SiNTs. The most important orientations and corresponding potential energy curves for both hydrogen and methane adsorption on the hollow sites are illustrated in Figs. 2 and 3.

It is worthy to point out that a similar vertical orientation has also been observed for hydrogen adsorption on SiCNTs and CNTs (Mpourmpakis et al. 2006).

By inspecting carefully the curves shown in Fig. 3, we find that for both hydrogen and methane, increase in nanotube diameter results in decrease in binding energy. This has explicitly been attributed to the curvature effect (Kleiner and Eggert 2001). Additionally, since the interaction energies for interaction of CH_4 and H_2 with SiNTs are in the region of physisorption through the van der Waals interactions, and CH_4 is more polarizable than H_2, stronger CH_4–SiNT interactions are resulted.

2.2 Choice of an accurate potential equation

To employ the results obtained by ab initio calculations in the simulation of hydrogen and methane adsorption on SiNTs, we require to choose a potential function as a link between ab initio calculations and canonical Monte Carlo simulations. The proper choice of this function is of crucial importance, because the accuracy of the simulation results is influenced by this choice. Therefore, three models of potential functions including (12-6) and (9-6) Lennard–Jones (LJ) and Morse equations were selected to describe the potential curves obtained from the first-principle calculations.

Neither (12-6) LJ nor (9-6) LJ equation could be fitted with the H_2 and CH_4 potential curves, because the slope of repulsion branch in LJ potentials is sharper than that in the potential curves from ab initio calculations, whereas we found that the Morse potential in (1) is in excellent coincidence with the results driven from the ab initio calculations for both hydrogen and methane, due to slower slope in the repulsion branch. The Morse potential is represented as follows (Lan et al. 2008):

$$U_i = 2D[X^2 - 2X], \quad X = \exp\left(-\frac{g}{2}\left(\frac{r_i}{r_e} - 1\right)\right) \tag{1}$$

where r_i is center to center distance (Å). For hydrogen and methane, the Morse potential parameters are listed in Table 1.

All the calculations have already been reported for adsorption of hydrogen on the surface of silicon nanotubes by Lan et al. (2008). It should be noted that our findings are consistent with their results.

2.3 Canonical Monte Carlo (CMC) simulation

A standard CMC simulation was carried out to investigate the adsorption of pure hydrogen and methane, and their mixture on SiNTs at different pressures, temperatures, and tube diameters. In this method, the standard procedure Metropolis sampling was applied for the acceptance decision of every configuration generated by the random displacement of a molecule from former configuration. For each isotherm point, 5×10^7 configurations were generated. The system was achieved to equilibrate after 2×10^7 steps, and the remaining 3×10^7 configurations were used to obtain ensemble average values for thermodynamic properties. The periodic boundary condition was imposed in the all three dimensions (Lan et al. 2008).

The intermolecular interactions between H_2–H_2 and CH_4–CH_4 were calculated using the (12-6) LJ potential (Lan et al. 2008; Heyden et al. 2002)

$$\phi_{\mathrm{LJ}}(r) = 4\varepsilon_{ff}\left[\left(\frac{\sigma_{ff}}{r}\right)^{12} - \left(\frac{\sigma_{ff}}{r}\right)^{6}\right]. \tag{2}$$

Here r is the distance between two interacting fluid molecules, σ_{ff} denotes the LJ fluid–fluid collision diameter in the unit of nm, and ε_{ff} is the LJ fluid–fluid potential well depth in the unit of K. Additionally, Lorentz–Berthelot combining rules in (3) were applied for the interaction between H_2 and CH_4 as well as the interaction of H_2 and CH_4 with (8, 8) CNT

$$\varepsilon_{ij} = \sqrt{\varepsilon_i \varepsilon_j}, \qquad \sigma_{ij} = \frac{1}{2}(\sigma_i + \sigma_j). \tag{3}$$

The Lennard–Jones parameters for each species are listed in Table 2.

The total interactions between adsorbed molecules and SWSiNTs were represented using the Morse potential equation, which was introduced before.

In the CMC simulation, the temperature, the volume of simulation box, and the number of molecules are held constant during the simulation of every state. In this work, the simulation box (100 Å × 100 Å × 45 Å) contains one single-walled nanotube with the length of about 37 Å at its center along with z-axis. The Virial equation of state with second and third viral coefficients was applied to estimate the number of fluid molecules at different temperatures and pres-

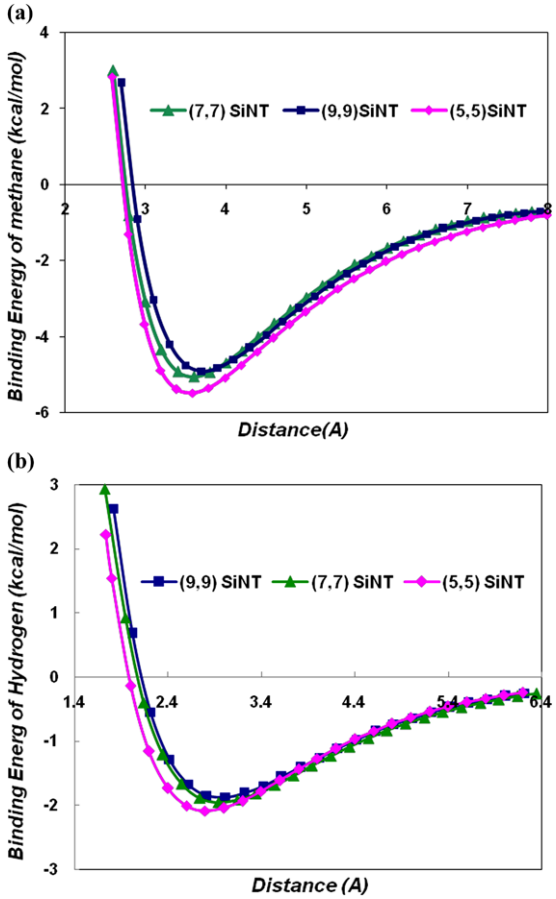

Fig. 3 Potential energy curves of H_2 and CH_4 adsorption on three different sizes of SiNTs with favorable orientation approaching the hollow sites: (**a**) methane adsorption (**b**) hydrogen adsorption

Table 2 Lennard–Jones parameters used in the simulations (Lan et al. 2008; Heyden et al. 2002)

Species	$\varepsilon/k_B(K)$	$\sigma(A)$
H_2–H_2	42.8	2.97
CH_4–CH_4	148.1	3.81
C–C	28	3.4

Table 1 The Morse potential parameters used to describe the interactions of H_2 and CH_4 with the hollow sites of the SiNTs

Interaction energies between gases and outside the tube walls						
Morse potential parameter	For (9, 9) SiNT		For (7, 7) SiNT		For (5, 5) SiNT	
	H_2	CH_4	H_2	CH_4	H_2	CH_4
D (kcal/mol)	1.1	2.951	0.983	2.603	0.973	2.548
g	4.83	5.71	4.768	5.703	4.98	5.818
$r_e(A)$	2.79	3.608	2.98	3.647	2.944	3.744

Table 3 Coefficients of temperature correlation for pure-component second Virial coefficients (Estela-Uribe et al. 2003)

Interaction	$b_{ij0} \times 10^{-2}$ ($dm^3\ mol^{-1}$)	b_{ij1} ($dm^3\ Kmol^{-1}$)	b_{ij2} ($dm^3\ K^2\ mol^{-1}$)
CH_4–CH_4	4.218856	-1.713109×10^1	-2.457425×10^3
H_2–H_2	2.083580	−1.928868	−1.065080

Table 4 Coefficients of temperature correlation for pure-component third Virial coefficients (Estela-Uribe et al. 2003)

Interaction	c_{ij0} ($dm^6\ mol^{-2}$)	c_{ij1} ($dm^6\ K\ mol^{-2}$)	c_{ij2} ($dm^6\ K^2\ mol^{-2}$)
CH_4–CH_4–CH_4	2.799668×10^{-3}	-9.276054×10^{-1}	2.446528×10^2
H_2–H_2–H_2	1.597000×10^{-4}	6.427210×10^{-2}	-1.254470×10^{-1}

Table 5 Coefficients of temperature correlation for interaction second Virial coefficients fitted to binary-mixture compression factors (Estela-Uribe et al. 2003)

Interaction	$b_{ij0} \times 10^{-2}$ ($dm^3\ mol^{-1}$)	b_{ij1} ($dm^3\ K\ mol^{-1}$)	$b_{ij2} \times 10^1$ ($dm^3\ K^2\ mol^{-1}$)
CH_4–H_2	3.733621	−9.050586	−5.118172

Table 6 Coefficients of temperature correlation for independent double-interaction third Virial coefficients fitted to binary-mixture compression factors (Estela-Uribe et al. 2003)

Interaction	$c_{ij0} \times 10^{-4}$ ($dm^6\ mol^{-2}$)	$c_{ij1} \times 10^{-1}$ ($dm^6\ K\ mol^{-2}$)	c_{ij2} ($dm^6\ K^2\ mol^{-2}$)
CH_4–CH_4–H_2	2.894530	2.082070	1.959194×10^1
CH_4–H_2–H_2	2.608140	1.182288	1.565030

sures to achieve more accurate results than usage ideal gas equation

$$\frac{PV}{NRT} = 1 + B'(T)P + C'(T)P^2,$$
$$B' = \frac{B}{RT}, \qquad C' = \frac{(C - B^2)}{(RT)^2}, \tag{4}$$

where B and C are the second and third Virial coefficients, respectively, which are functions of temperature and type of species. Virial coefficients were determined through following relations reported by J.F. Estela-Uribe et al. (2003)

$$B_{ij} = b_{ij,0} + \frac{b_{ij,1}}{T} + \frac{b_{ij,2}}{T^2}, \tag{5}$$

$$C_{ijk} = c_{ijk,0} + \frac{c_{ijk,1}}{T} + \frac{c_{ijk,2}}{T^2}. \tag{6}$$

The amounts of the coefficients in (5) and (6) for pure H_2 and CH_4 are listed in Tables 3 and 4 (Estela-Uribe et al. 2003).

Furthermore, temperature and type of molecule, for the mixture of gases B and C, are also dependent on the bulk composition through the following relations:

$$B_{\mathrm{MIX}} = \sum_i \sum_j x_i x_j B_{ij}, \tag{7}$$

$$C_{\mathrm{MIX}} = \sum_i \sum_j \sum_k x_i x_j x_k C_{ijk}. \tag{8}$$

In (7) and (8), x_i, x_j, and x_k are the mole fractions of the ith, jth, and kth components of the mixture. B_{ij} and C_{ijk} are also obtained by (5) and (6), and the corresponding parameters are listed in Tables 5 and 6 (Estela-Uribe et al. 2003).

Furthermore, to obtain adsorption isotherms, gravimetric storage capacity (pw) was calculated using following equation:

$$\rho_W = \frac{N_{\mathrm{gas}}.m_{\mathrm{gas}}}{N_{\mathrm{gas}}.m_{\mathrm{gas}} + N_{\mathrm{si}}.m_{\mathrm{si}}}. \tag{9}$$

Here, N_{gas} and N_{Si} are the number of adsorbed molecules and nanotube atoms, respectively.

In addition, the heat of combustion was used to evaluate the volumetric energy storage; the corresponding values for methane and hydrogen are −55.6 MJ/kg and −141.789 MJ/kg, respectively (Kowalczyk et al. 2007).

3 Results and discussion

3.1 Adsorption of pure H_2 and CH_4 on SiNTs

The adsorption behaviors of CH_4 and H_2 on three different sizes of SiNTs including (5, 5), (7, 7), and (9, 9) SiNTs were investigated at two supercritical temperatures (293 K, 313 K) and pressures ranging from 1 up to 10 MPa.

Our simulation results in Fig. 4 reveal that for hydrogen and methane adsorption, the gravimetric storage capacity is an increasing function of pressures and decreasing function of temperatures. As expected, in all the simulations, the amount of CH_4 adsorption capacity is greater than H_2, due to its stronger interaction with SiNTs and higher boiling temperature.

The effect of tube size on the adsorption capacity was also investigated. As mentioned above, we perceived from the ab initio calculations that the potential interaction of fluids with SiNTs increase palpably for both hydrogen and methane adsorption, while the diameter declines. However,

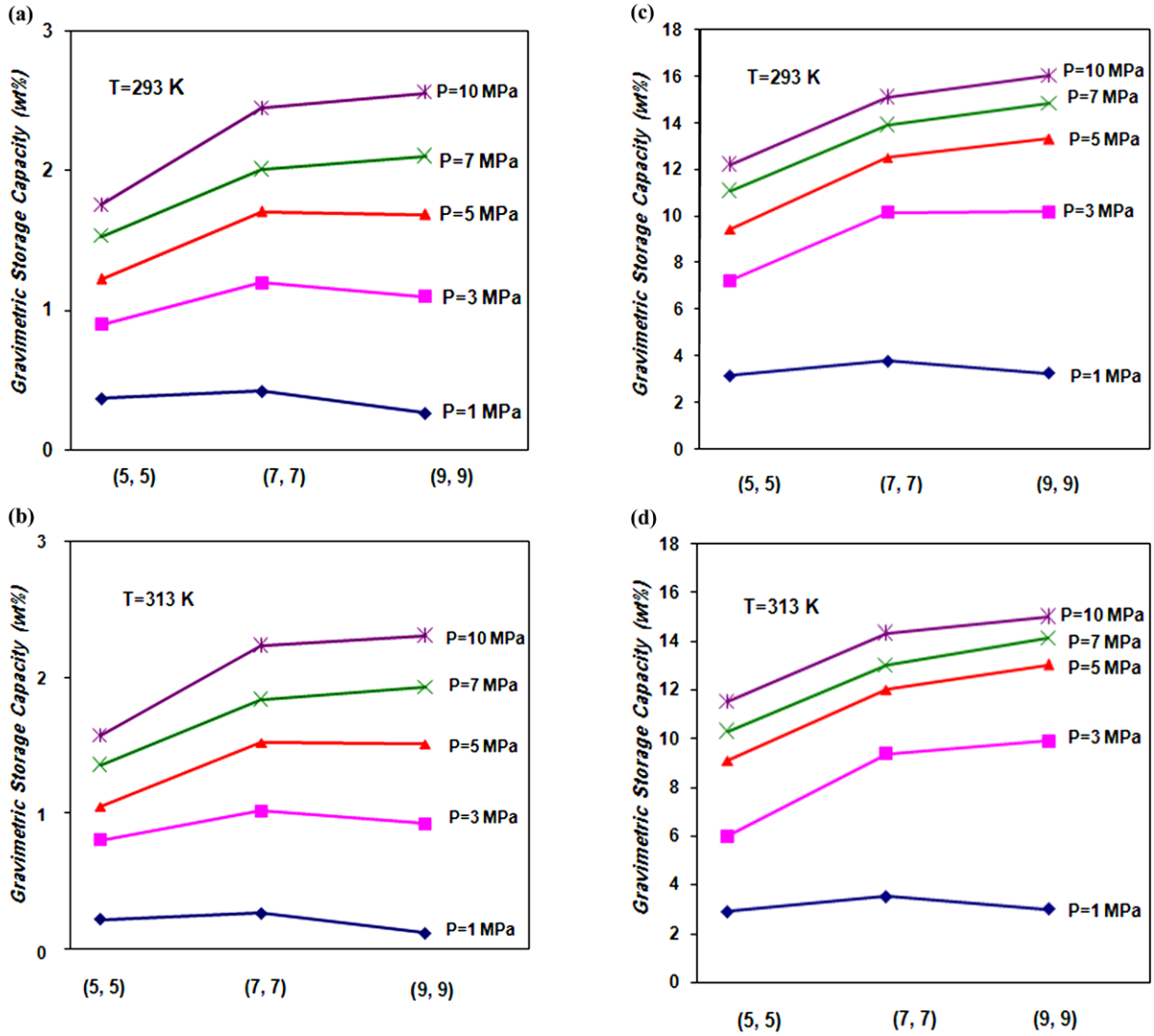

Fig. 4 Gravimetric adsorption isotherms for adsorption of H_2 and CH_4 on the (5, 5), (7, 7), and (9, 9) SiNTs at 293 K and 313 K, and five pressures: (**a**) H_2 adsorption at 293 K (**b**) H_2 adsorption at 313 K (**c**) CH_4 adsorption at 293 K (**d**) CH_4 adsorption at 313 K

our CMC simulation results in Fig. 4 indicate that among the three different sizes of silicon nanotubes, the (7, 7) and (9, 9) SiNTs provide the highest storage capacity for both H_2 and CH_4 within the pressure range under study. This inconsistency emanate from the fact the amount of gas adsorption is influenced by several factors such as the space, surface area, and attractive force. The co-effect of these factors determines the magnitude of fluid adsorption on the SiNTs (Gu et al. 2002).

The smaller space and surface area of the (5, 5) SiNTs overwhelm the higher potential interaction of CH_4 and H_2 with this sorbent. Therefore, over the pressure range under study, the (5, 5) SiNT exhibits the lowest gravimetric storage capacity for both H_2 and CH_4 compared to (7, 7) and (9, 9) SiNTs.

3.2 Comparison of H_2 and CH_4 adsorption on the SiNTs and CNTs

Figure 5 depicts the gravimetric storage capacity for H_2 and CH_4 adsorption on the (5, 5) SiNTs and isodiameter (8, 8) CNTs as a function of pressure at 293 K. All the hydrogen and methane adsorption isotherms are characterized by type 1 (Langmuir shape), and no capillary condensation is observed.

As we can see from this figure, due to stronger interaction between the SiNTs and fluids, the values of hydrogen and methane adsorption on the (5, 5) SiNTs are considerably higher than those on the isodiameter (8, 8) CNTs. The gravimetric percentage enhancement for both H_2 and CH_4 are presented in Table 7.

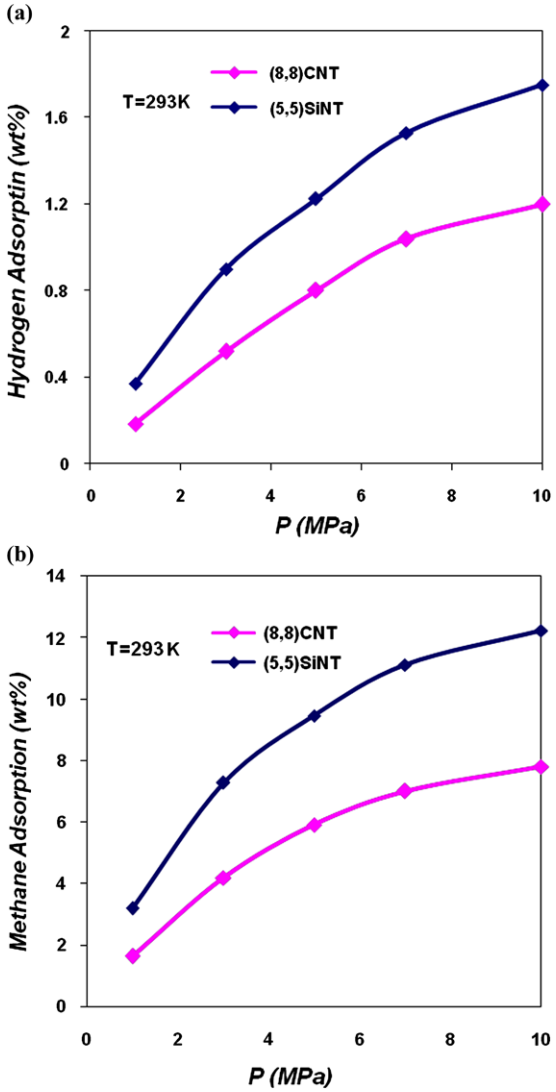

Fig. 5 Gravimetric storage capacity for adsorption of H_2 and CH_4 on the (5, 5) SiNTs compared to isodiameter (8, 8) CNTs at 293 K and pressure range from 1 to 10 MPa: (**a**) H_2 gravimetric capacity and (**b**) CH_4 gravimetric capacity

Moreover, the adsorption isotherms for hydrogen and methane do not show saturation. Therefore, higher adsorption capacity for both H_2 and CH_4 is expected by further increase in pressure (Li and Yang 2005). Additionally, increase in pressure results in increase in repulsion force. Because, in contrary to the LJ potential applied to describe gas adsorption on the CNTs, the Mors potential rises smoothly at repulsion branch, the enhancement rate of gas adsorption on the SiNTs is greater than that in the CNTs at elevated pressures. Therefore, we can conclude that the SiNTs are a promising candidate for hydrogen storage to achieve the DOE target (Lan et al. 2008).

Moreover, in order to answer the question, whether SiNTs are appropriate media for methane adsorption, the

Table 7 Gravimetric percentage enhancement of H_2 and CH_4 adsorption on the (5, 5) SiNTs compared to (8, 8) CNTs at 293 K

Adsorbed molecules	1 MPa	3 MPa	5 MPa	7 MPa	10 MPa
CH_4	101%	73%	53%	47%	45%
H_2	95%	74%	60%	59%	57%

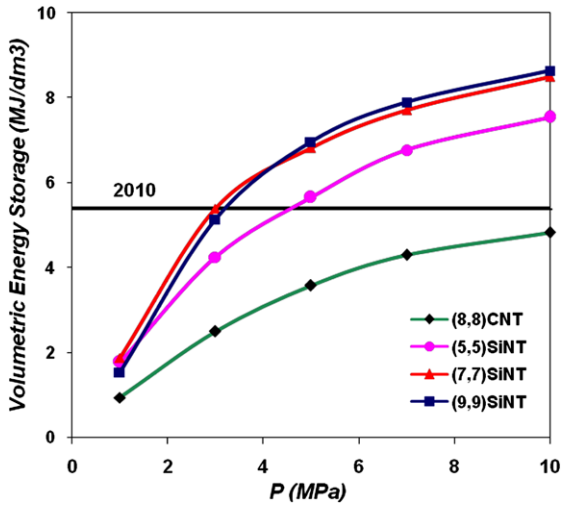

Fig. 6 The variation of stored volumetric energy for adsorption of methane on the (5, 5), (7, 7), and (9, 9) SiNTs as well as (8, 8) CNTs with pressure at 298 K. *Solid line* indicates the US Freedom CAR Partnership goal (5.4 MJ/dm^3)

stored volumetric energy for adsorption of methane on the SiNTs has been presented in Fig. 6.

The methane fluid requires to be compressed to approximately 13 MPa at 293 K, to provide the 2010 target for volumetric energy storage (5.4 MJ/dm^3) (Kowalczyk et al. 2006), whereas all the three silicon nanotubes investigated in this work achieved this goal at much lower pressures. Furthermore, since the interaction energies of methane with the SiNTs are in the region of physisorption, captured methane can simply be liberated by variation of the temperature. Therefore, we can conclude that silicon nanotubes are excellent materials for methane storage at ambient temperatures. In comparison with the (5, 5) SiNTs, isodiameter (8, 8) CNTs can not provide the 2010 target over the pressure range under study.

3.3 Adsorption of CH_4 and H_2 mixture on the SiNTs

For all considered SiNTs, the gravimetric storage capacity of two components of equimolar CH_4–H_2 mixture is illustrated in Fig. 7. The temperature was set at 293 K. As we can observe, the variation patterns of H_2 and CH_4 adsorption on

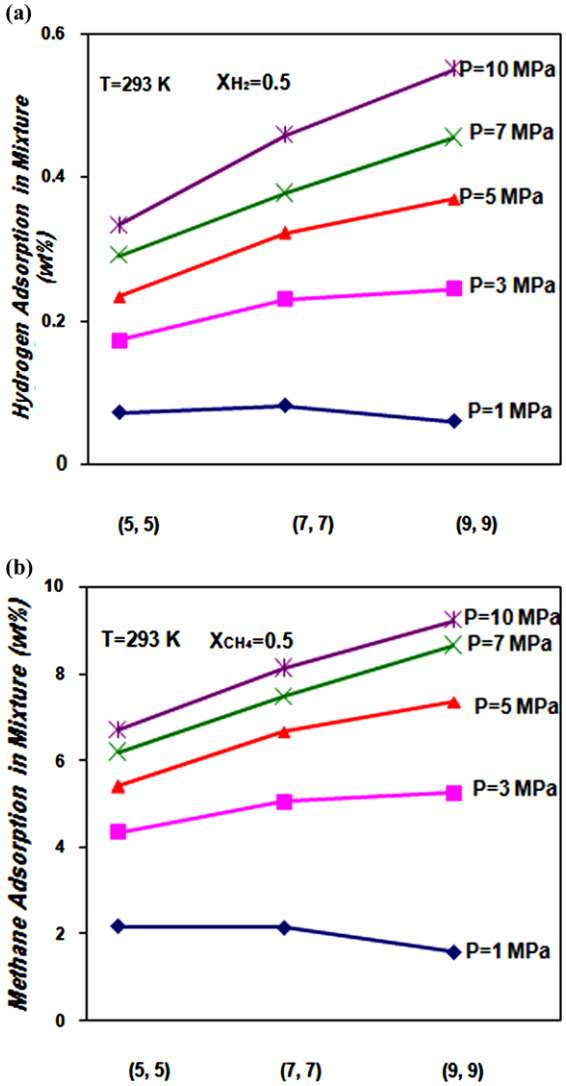

Fig. 7 Pressure variation of gravimetric adsorption isotherms of hydrogen and methane in the equimolar CH_4–H_2 mixture at 293 K: (**a**) hydrogen isotherms and (**b**) methane isotherms

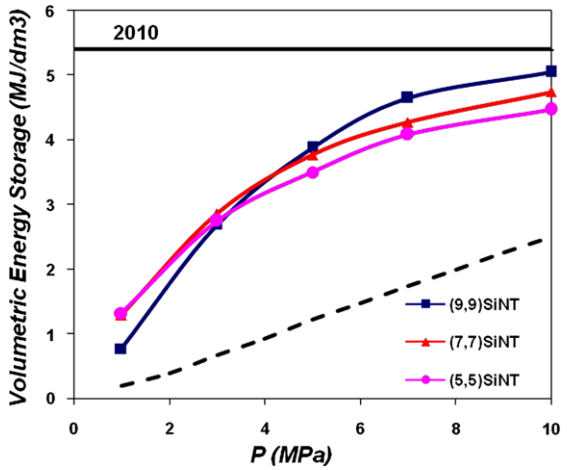

Fig. 8 The stored volumetric energy of equimolar H_2–CH_4 mixture in the different sizes of SiNTs versus storage pressure at 293 K. *Solid line* corresponds to the 2010 target of the US Freedom CAR Partnership (5.4 MJ/dm^3) and *dashed line* corresponds to the volumetric energy of H_2–CH_4 compression in the equimolar mixture

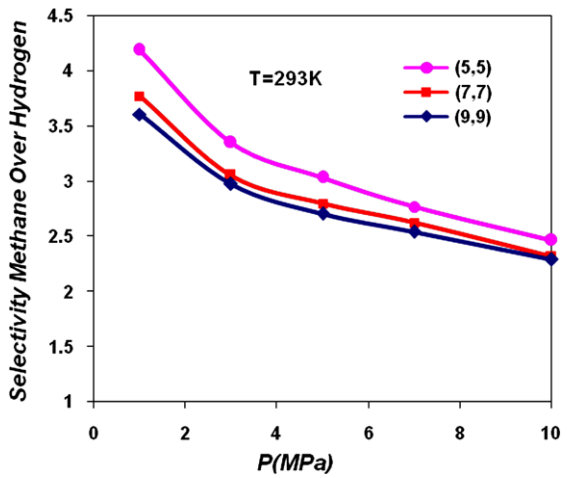

Fig. 9 The variation of equilibrium selectivity of methane over hydrogen in the (5, 5), (7, 7), and (9, 9) SiNTs with pressure

binary mixture with pressure and temperature is similar to their pure adsorption.

Additionally, it is clear from Fig. 8 that the amount of volumetric energy stored by adsorption of equimolar CH_4–H_2 mixture on the SiNTs is much higher than that by bulk compression. Furthermore, the stored volumetric energy of equimolar mixture for adsorption on the (9, 9) SiNTs at 10 MPa is very close to the US Freedom CAR Partnership goal by 2010.

3.4 Selectivity

The discrepancies between the adsorption behaviors for adsorption of CH_4 and H_2 molecules on the SiNTs manifesting these sorbents are effective for separation of CH_4 and H_2 from each other.

To provide deep insight into the separation efficiency of silicon nanotubes, we can explain the equilibrium selectivity of CH_4 over H_2 as follows (Morales-Cas et al. 2007):

$$S_{CH_4,H_2} = \frac{(x_{CH_4}/x_{H_2})_{pore}}{(y_{CH_4}/y_{H_2})_{bulk}} \tag{10}$$

where x and y refer to the mole fractions of species at adsorbent and bulk phases, respectively. It is worthy to point out that if the selectivity is larger than unity, methane is preferentially adsorbed compared to hydrogen.

In this section we consider, how pressure and tube diameter exert their affects on the selectivity of CH_4 over H_2 in the equimolar mixture and at 293 K.

Figure 9 displays the equilibrium selectivity for CH_4 over H_2 storage on the SiNTs versus storage pressure. Obviously,

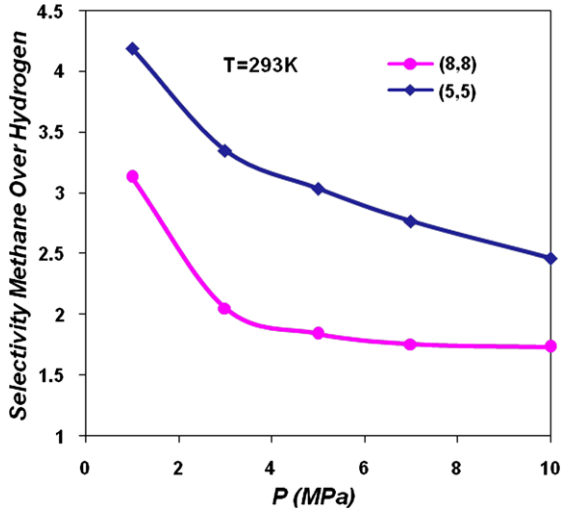

Fig. 10 The equilibrium selectivity of methane over hydrogen in the (5, 5) SiNTs and (8, 8) CNTs

the equilibrium selectivity diminishes as the pressure increases. This phenomenon is attributed to the packing effect which becomes dominant at elevated pressures. Therefore, in these conditions, the smaller molecules are more proper to be packed in the nanotubes (Gu et al. 2002).

In addition, the value of the selectivity mostly is influenced by the potential interaction between fluids and SiNTs (Huang et al. 2007). Since the interaction energy of CH_4 and H_2 with SiNTs come nearer to each other with increase in the tube diameter, the (9, 9) SiNT indicates the lowest value of equilibrium selectivity.

The variation of selectivity with pressure in the (5, 5) SiNTs compared to the isodiameter (8, 8) CNTs was also presented in Fig. 10. The results show that the (8, 8) SiNT is more favorable than the (8, 8) CNT for separation of CH_4 and H_2 from each other.

It is worthy to point out that in all the cases, the selectivity of CH_4 over H_2 is higher than unity. Therefore, the separation of these gases is possible under the investigated conditions.

4 Conclusions

In summary, the performance of silicon nanotubes as a novel material for pure and mixed H_2 and CH_4 adsorption as well as their separation in the equimolar mixture were studied using a multiscale theoretical approach. The interaction energies of hydrogen and methane with the SiNTs determined via ab initio calculations were fitted to a Morse potential equation employed as an input in the canonical Monte Carlo simulations. To investigate the effects of size, temperature, and pressure on the adsorption and separation behaviour of hydrogen and methane, three different-sized silicon nanotubes including (5, 5), (7, 7), and (9, 9) SiNTs, two temperatures (293 and 313 K), and five pressures in the range from 1 to 10 MPa were considered. In all the investigated conditions, the adsorption capacities for adsorption of both H_2 and CH_4 on the SiNTs are increasing function of pressure and decreasing function of temperature. Additionally, simulation results indicate that higher adsorption capacity for both H_2 and CH_4 are provided by SiNTs compared to CNTs. This phenomenon arises from the fact that electronic cloud around the surface of silicon nanotube is denser than that around the CNT, which results in stronger VDW attraction to the gases. As an excellent result from this research, in all three sizes of SiNTs, the amount of energy stored by CH_4 adsorption exceeds the target of the US Freedom CAR Partnership by 2010 at 293 K and low pressures from 3 to 4.5 MPa. This target can not be achieved by methane compression at such low pressures. Moreover, the interaction energies of methane with the SiNTs are in the regain of physisorption. Therefore, liberation of methane can be controlled by simple variation in the temperature. Accordingly, we can conclude that the SiNTs are appropriate materials for methane storage. Furthermore, the stored volumetric energy of equimolar mixture in the (9, 9) SiNT at 10 MPa is very close to the US Freedom CAR Partnership target.

Moreover, the possible usage of silicon nanotubes as an efficient media for separation of hydrogen and methane in the equimolar mixture were explored at 293 K and pressure range from 1 to 10 MPa. The results indicate that the selectivity is a decreasing function of pressure because the packing effect is principle at higher pressures. Regarding the amounts of selectivity of methane over hydrogen, we can conclude that although all three investigated SiNTs are suitable medias for H_2 and CH_4 separation, the (5, 5) SiNT is the best one, in which the selectivity varies from 2.5 to 4.2 at the pressure range under study.

References

Bekyarova, E., Murata, K., Yudasaka, M., Kasuya, D., Iijima, S., Tanaka, H., Kahoh, H., Kaneko, K.: Single-wall nanostructured carbon for methane storage. J. Phys. Chem. B **107**, 4681–4684 (2003)

Bhatia, S.K., Myers, A.L.: Optimum conditions for adsorptive storage. Langmuir **22**, 1688–1700 (2006)

Cao, D., Wang, W., Duan, X.: Grand canonical Monte Carlo simulation for determination of optimum parameters for adsorption of supercritical methane in pillared layered pores. J. Colloid Interface Sci. **254**, 1–7 (2002)

Cao, D., Zhang, X., Chen, J., Wang, W., Yun, J.: Optimization of single-walled carbon nanotube arrays for methane storage at room temperature. J. Phys. Chem. B **107**, 13286–13292 (2003)

Chen, H., Sholl, D.S.: Predictions of selectivity and flux for CH_4/H_2 separations using single walled carbon nanotubes as membranes. J. Membr. Sci. **269**, 152–160 (2006)

Chen, Y.W., Tang, Y.H., Pei, L.Z., Guo, C.: Self-assembled silicon nanotubes grown from silicon monoxide. Adv. Mater. **17**, 564–567 (2005)

Cote, A.P., Benin, A.I., Ockwig, N.W., O'Keeffe, M., Matzger, A.J., Yaghi, O.M.: Porous, crystalline, covalent organic framework. Science **310**, 1166–1170 (2005)

Dillon, A.C., Jones, K.M., Bekkedahl, T.A., Kiang, C.H., Bethune, D.S., Heben, M.J.: Storage of hydrogen in single-walled carbon nanotubes. Nature **386**, 377–379 (1997)

Estela-Uribe, J.F., Jaramillo, J., Salazar, M.A., Trusler, J.P.M.: Virial equation of state for natural gas systems. Fluid Phase Equilib. **204**, 169–182 (2003)

Gu, C., Gao, G.-H., Yu, Y.-X., Nitta, T.: Simulation for separation of hydrogen and carbon monoxide by adsorption on single-walled carbon nanotubes. Fluid Phase Equilib. **194–197**, 297–307 (2002)

Heyden, A., Düren, T., Keil, J.F.: Study of molecular shape and non-ideality effects on mixture adsorption isotherms of small molecules in carbon nanotubes: a grand canonical Monte Carlo simulation study. Chem. Eng. Sci. **57**, 2439–2448 (2002)

Huang, L., Zhang, L., Shao, Q., Lu, L., Lu, X., Jiang, S., Shen, W.: Simulations of binary mixture adsorption of carbon dioxide and methane in carbon nanotubes: temperature, pressure, and pore size effects. J. Phys. Chem. C **111**, 11912–11920 (2007)

Kleiner, A., Eggert, S.: Curvature, hybridization, and STM images of carbon nanotubes. Phys. Rev. B **64**, 113402 (2001)

Kowalczyk, P., Solarz, L., Do, D.D., Samborski, A., MacElroy, J.M.D.: Nanoscale tubular vessels for storage of methane at ambient temperatures. Langmuir **22**, 9035–9040 (2006)

Kowalczyk, P., Brualla, L., Zywociński, A., Bhatia, S.K.: Single-walled carbon nanotubes: efficient nanomaterials for separation and on-board vehicle storage of hydrogen and methane mixture at room temperature? J. Phys. Chem. C **111**, 5250–5257 (2007)

Lan, J., Cheng, D., Cao, D., Wang, W.: Silicon nanotube as a promising candidate for hydrogen storage: from the first principle calculations to grand canonical Monte Carlo simulations. J. Phys. Chem. C **112**, 5598–5604 (2008)

Lee, J.-W., Kang, H.-C., Shim, W.-G., Kim, C., Moon, H.: Methane adsorption on multi-walled carbon nanotube at (303.15, 313.15, and 323.15) K. J. Chem. Eng. Data **51**, 963–967 (2006)

Li, Y., Yang, R.T.: Significantly enhanced hydrogen storage in metal-organic frameworks via spillover. J. Am. Chem. Soc. **128**, 726–727 (2005)

Li, Y., Yang, R.T.: Hydrogen storage in metal-organic frameworks by bridged hydrogen spillover. J. Am. Chem. Soc. **128**, 8136–8137 (2006)

Lithoxoos, G.P., Samios, J., Carissan, Y.: Investigation of silicon model nanotubes as potential candidate nanomaterials for efficient hydrogen storage: a combined ab initio/grand Canonical Monte Carlo simulation study. J. Phys. Chem. C **112**, 16725–16728 (2008)

Meng, T.D., Wang, C.-Y., Wang, S.-Y.: First-principles study of a single Ti atom adsorbed on silicon carbide nanotubes and the corresponding adsorption of hydrogen molecules to the Ti atom. Chem. Phys. Lett. **437**, 224–228 (2007)

Morales-Cas, A.M., Moya, C., Coto, B., Vega, L.F., Calleja, G.: Adsorption of hydrogen and methane mixtures on carbon cylindrical cavities. J. Phys. Chem. C **111**, 6473–6480 (2007)

Mpourmpakis, G., Froudakis, G.E., Lithoxoos, G.P., Samios, J.: SiC nanotubes: a novel material for hydrogen storage. Nano Lett. **6**, 1581–1583 (2006)

Ohkubo, T., Miyawaki, J., Kaneko, K., Ryoo, R., Seaton, N.A.: Adsorption properties of templated mesoporous carbon (CMK-1) for nitrogen and supercritical methane experiment and GCMC simulation. J. Phys. Chem. B **106**, 6523–6528 (2002)

Peng, X., Cao, D., Wang, W.: Heterogeneity characterization of ordered mesoporous carbon adsorbent CMK-1 for methane and hydrogen storage: GCMC simulation and comparison with experiment. J. Phys. Chem. C **112**, 13024–13036 (2008)

Poirier, E., Chahine, R., Benard, P., Lafi, L., Dorval-Douville, G., Chandonia, P.A.: Hydrogen adsorption measurements and modeling on metal-organic frameworks and single-walled carbon nanotubes. Langmuir **22**, 8784–8789 (2006)

Rosi, N.L., Eckert, J., Eddaoudi, M., Vodak, D.T., Kim, J., O'Keeffe, M., Yaghi, O.M.: Hydrogen storage in microporous metal-organic frameworks. Science **300**, 1127–1129 (2003)

Roussel, T., Pellenq, R.J.M., Bienfait, M., Vix-Guterl, C., Gadiou, R., Beguin, F., Johnson, M.: Thermodynamic and neutron scattering study of hydrogen adsorption in two mesoporous ordered carbons. Langmuir **22**, 4614–4619 (2006)

Ryou, J., Hong, S., Kim, G.: Hydrogen adsorption on hexagonal silicon nanotubes. Solid State Commun. **148**, 469–471 (2008)

Sha, J., Niu, J., Ma, X., Xu, J., Zhang, X., Yang, Q., Yang, D.: Silicon nanotubes. Adv. Mater. **14**, 1219–1221 (2002)

Tanaka, H., Kanoh, H., Yudasaka, M., Iijima, S., Kaneko, K.: Quantum effects on hydrogen isotope adsorption on single-wall carbon nanohorns. J. Am. Chem. Soc. **127**, 7511–7516 (2005)

Tang, Y.H., Pei, L.Z., Chen, Y.W., Guo, C.: Self-assembled silicon nanotubes under supercritically hydrothermal conditions. Phys. Rev. Lett. **95**, 116102 (2005)

Yaghi, O.M., O'Keeffe, M., Ockwig, N.W., Chae, H.K., Eddaoudi, M., Kim, J.: Reticular synthesis and the design of new materials. Nature **423**, 705–714 (2003)

Zhang, Y.: Computational study of the transport mechanisms of molecules and ions in solid materials. Dissertation, Texas A&M University, Texas, USA (2006)

Zhou, L., Sun, Y., Yang, Z., Zhou, Y.: Hydrogen and methane sorption in dry and water-loaded multiwall carbon nanotubes. J. Colloid Interface Sci. **289**, 347–351 (2005)